International Journal of Thermophysics, Vol. 23, No. 4, July 2002 (© 2002)

Effects of Surface Morphology and Composition Modification on Spectral Emissivity and Thermal Diffusivity Profile at High Temperatures[1]

Y. W. Kim[2]

A new all-spectroscopic method for depth-resolved thermal diffusivity measurement of metallic specimens has been demonstrated. The method entails measurement of the mass entrained into a laser-produced plasma (LPP) plume in such a manner that the plume is representative of the specimen in elemental composition. Both the abundance of matter and its elemental composition are measured by time-resolved spectroscopy for each LPP plume. In order to delineate the morphology versus composition basis of the depth dependence, a new study on a Nichrome ribbon specimen heated by ohmic heating in a vacuum is presented. A set of depth-resolved thermal diffusivity measurements is carried out, while noting the attendant changes in the spectral emissivity and elemental composition at succeeding ablation layers. Additional measurements are carried out after the specimen has been treated under varying heating conditions. Preferential diffusion of chromium at high temperatures has been found to contribute to the dynamics of surface thermophysical properties at high temperatures. Representative LPP ablation is well suited for removal of surface impurities prior to thermophysical property measurements by the pulse heating technique.

KEY WORDS: depth profile of elemental composition; emissivity; laser-produced plasmas; Nichrome ribbon; surface contaminants; thermal diffusivity.

[1] Paper presented at the Fourteenth Symposium on Thermophysical Properties, June 25–30, 2000, Boulder Colorado, U.S.A.

[2] Department of Physics, Lewis Laboratory #16 Lehigh University, Bethlehem, Pennsylvania 18015-3182, U.S.A. E-mail: ywk0@lehigh.edu

0195-928X/02/0700-1103/0 © 2002 Plenum Publishing Corporation

1. INTRODUCTION

It has been shown that excitation of a multi-element condensed-phase material surface by a tailored high-power laser pulse can produce dense plasmas which are representative of the target matter in elemental composition [1–4]. The plasma of the same composition as the bulk is uniquely definable. The criterion for a representative LPP plume is to drive the movement of the target surface by ablation in pace with the thermal diffusion front that propagates into the interior of the bulk.

The criterion for representative plasma production provides the measurement opportunity for thermal diffusivity because the mass entrained into the plasma plume is governed by the thermal diffusivity of the specimen. We have further shown that the mass loss can be measured either by the impulse imparted on the target [5, 6] or by time-resolved spectroscopy of the LPP plume [7–9]. Since the elemental composition of the plume is determinable at the same time [3, 4] in either implementation, it has become in principle possible to uniquely attribute the thermophysical properties to the composition of the material.

The amount of matter ablated from the surface results from a competition of surface heating, phase transitions leading to vapor production, dispersal of the plasma matter by diffusion and hydrodynamic processes, and thermal diffusion into the bulk. We have shown [9] that these competing processes can be parameterized by three physical attributes of the constituent players in the form of a scaling relationship:

$$\theta = C D_{\mathrm{T}}^{\alpha} M^{\beta} H_{\mathrm{f}}^{\gamma}. \tag{1}$$

Here θ denotes the thickness in cm, D_{T} the thermal diffusivity in $\mathrm{cm}^2 \cdot \mathrm{s}^{-1}$, M the molar mass, and H_{f} the heat of formation in $\mathrm{J} \cdot \mathrm{g}^{-1}$. $C = 11.07 \pm 0.45$, $\alpha = 0.91 \pm 0.01$, $\beta = -\alpha$, and $\gamma = -1$.

The purpose of this paper is to further investigate the manner in which the elemental composition and morphology of a material affect its thermal diffusivity. We have chosen a two-element alloy of 80Ni-20Cr Nichrome in the form of a ribbon, which is suitable for thermal cycling by ohmic heating to affect the morphology and elemental composition.

2. EXPERIMENTAL SETUP FOR A STUDY OF NICHROME RIBBON

The experimental setup is built around a small vacuum chamber consisting of a fused quartz cylinder. The specimen stage is implemented on a metal flange on one end, and a large-diameter fused quartz lens is mounted

on the opposite end. The specimen stage consists of two electrically insulated feedthroughs each with a conducting rod, which can be translated along, and rotated about, its axis. The metal flange can be rotated about the chamber axis for the purpose of aligning the specimen with respect to the laser beam and spectroscopic and imaging detectors outside. The vacuum chamber can be pumped down to 10^{-4} Pa.

A Q-switched Nd:YAG laser provides the laser pulses at required pulsed power density in the range of 10^9 to 10^{11} W·cm^{-2}. The laser beam and the detectors share the same lens mounted on the vacuum chamber by means of a dichroic mirror which reflects the laser pulse but transmits the LPP plume emissions over the entire near infrared to uv spectral range down to 200 nm.

The Nichrome specimen is 0.20 mm thick, 4.76 mm wide, and 45.09 mm long. The ribbon specimen is placed into position by clamping onto the two feedthrough electrodes. The Nichrome ribbon is heated to temperatures up to 1300 K.

The glowing surface of the Nichrome ribbon is imaged onto a gated CCD array detector with a 1024 by 256-pixel field of view. A two-dimensional digitized image of 16-bit intensity resolution is obtained upon gating of a microchannel plate intensifier covering the CCD detector.

In addition, the LPP plume is examined for elemental composition by means of time- and space-resolved spectroscopy. When such spectroscopic analyses are repeated, we obtain the depth profile of surface elemental composition. A spectrograph equipped with a second gated, intensified CCD array detector is used for this purpose.

The accumulated mass loss due to a preset set number of LPP ablations is independently measured by means of a digital microbalance. The measured mass loss by weighing of the specimen provides a calibration for the procedure of determining the total mass entrained into a LPP plume by spectroscopy. Once the calibration has been carried out, it is possible to measure the thickness of the surface layer removed by each LPP ablation without making physical contact with the specimen.

Figure 1 shows the image of the heated Nichrome ribbon. The white-light thermal emission intensity profiles at the center of the ribbon are displayed, one from a fresh surface with a single-ablation crater (Fig. 1a) and another around the same crater after 15 additional ablations moments later (Fig. 1b). The thermal emission intensity from the crater after one LPP ablation is reduced by 16.3% from that of the surrounding areas, suggesting that the emissivity of the freshly exposed surface is smaller than that of the undisturbed surface. However, the reduction in thermal emission intensity from the crater continues when additional LPP ablations are administered to the crater before leveling off at about 40%. The maximum

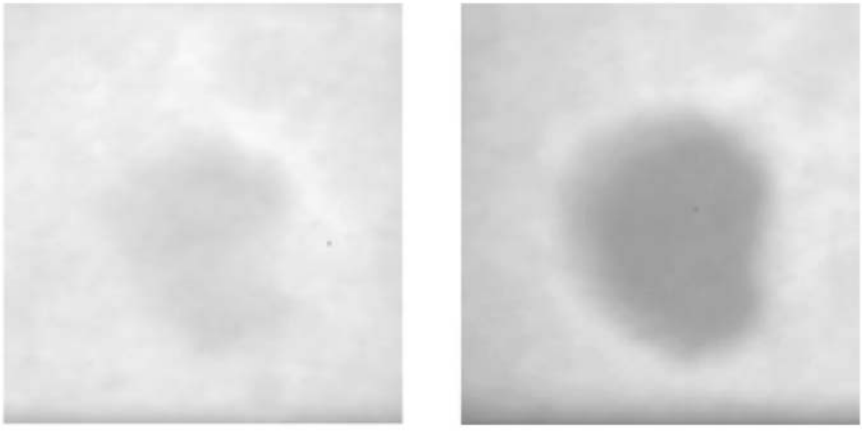

Fig. 1. White light images of the 3 mm × 3 mm area of a heated Nichrome ribbon with: (a) a crater of single LPP ablation and (b) the same crater with 15 additional ablations.

reduction of the thermal emission intensity is too large to be explained entirely by reductions in the emissivity, suggesting the existence of a depth-dependent temperature profile. We will examine this in detail in the next section.

3. DEPTH-RESOLVED ELEMENTAL COMPOSITION

Continued measurement by prolonged observation of the thermal emission intensity under a constant heating condition has revealed that the freshly exposed surface recovers over the next several minutes. This phenomenon was examined in two different ways. Firstly, spectroscopic analysis was carried out for the Nichrome ribbon at the elevated temperature by repetitively producing the LPP plumes from one surface layer after another. Secondly, a Nichrome ribbon was first aged, by heating it at constant power for 15 h in a vacuum. The surface was then analyzed at room temperature in comparison with a fresh Nichrome specimen.

Figure 2 shows a sequence of LPP plume spectra taken in rapid succession from the heated Nichrome ribbon. It is apparent that the elemental composition ceases to change with depth beyond the first few ablation layers, even though the thermal emission intensity continues to decrease over many more ablation layers. Figure 3 shows the two-dimensional contour plots of white light intensity for the two runs shown in Fig. 1.

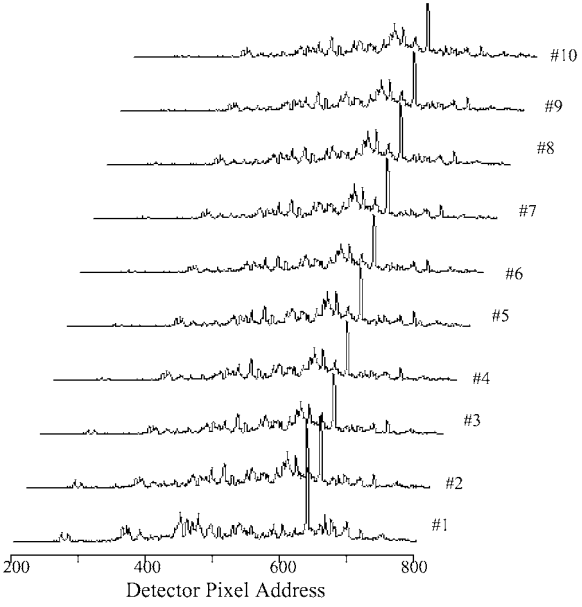

Fig. 2. LPP plume emission spectra of ten successive surface layers of a heated Nichrome ribbon at 1090 K in the order they were taken from #1 to #10. The spectral intensity is shown against wavelength, expressed in the array detector's pixel address. The wavelength range is from 330.5 nm (pixel 200) to 542.1 nm (pixel 800).

If we now allow some time for the ribbon to remain at the temperature, the relative concentration of chromium and nickel can be seen to fluctuate depending on the depth and duration of the period between successive LPP analyses. Immediately after an LPP ablation, the elemental composition of the base alloy is first seen, as shown in Fig. 2. But in short time, the surface is enriched in chromium by preferential diffusion, displacing nickel. This behavior is documented in Fig. 4. The depth profile of elemental composition of the fresh specimen (Fig. 4a) is contrasted to that of the thermally aged specimen (Fig. 4b). In the fresh specimen, the outermost surface layer is enriched with chromium but the elemental composition reaches that of the base alloy within three LPP ablations, i.e., approximately over a distance of 2 μm. In contrast, the thermally aged specimen reveals a much larger depth over which the composition varies. In 15 h of heating in a vacuum, the transition layer has thickened to more than 10 μm, and the base alloy composition has shifted slightly away from

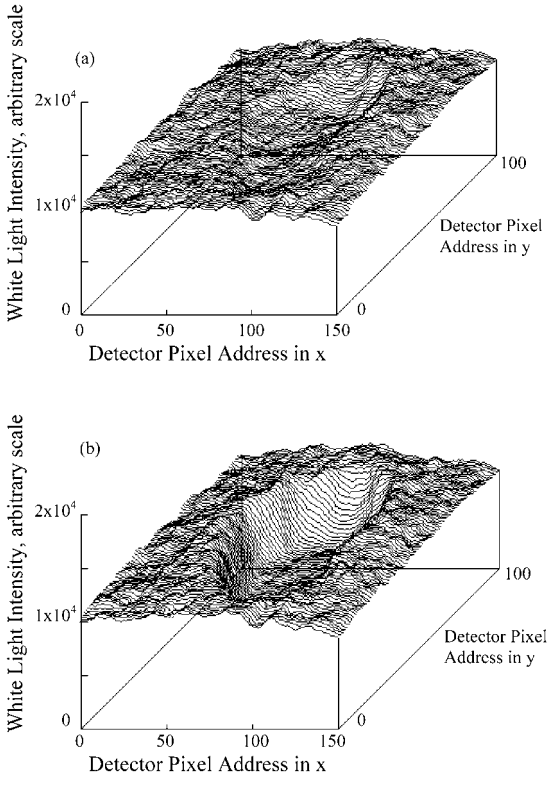

Fig. 3. White light intensity contour plots of the two images shown in Fig. 1a and 1b. A fresh Nichrome ribbon was heated to 1090 K and its surface was ablated by laser-produced plasmas: (a) 150×100-pixel area with a once ablated crater at the center and (b) the same area with the crater ablated 15 more times. The image pixels are spaced 0.04 mm in both x and y directions.

that of the fresh specimen. The average thickness of the ablation layers for a fresh Nichrome ribbon is 0.62 μm per laser pulse.

4. TEMPERATURE MEASUREMENT

The temperature of the Nichrome ribbon specimen is varied by changing the input power. The equilibrium temperature is a result of the radiative loss by blackbody radiation, latent heat of evaporation of the specimen matter, and thermal conduction of heat from the heated ribbon to the electrodes. Under a fixed heating condition, the rate of evaporative mass

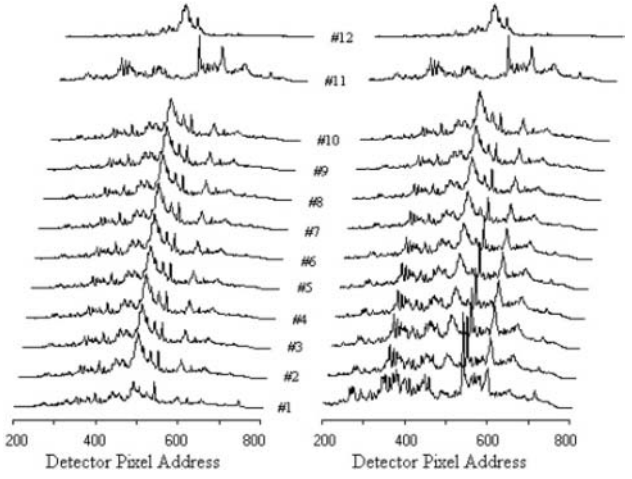

Fig. 4. Successive LPP spectra taken from: (a) a fresh Nichrome ribbon at room temperature and (b) an aged Nichrome ribbon at room temperature after 15 h of heating at 1090 K. Spectra #11 and #12 are from pure chromium and nickel, respectively. The wavelength range is from 330.5 nm (pixel 200) to 542.1 nm (pixel 800).

loss is measured by measuring the mass change of the ribbon specimen over a heating period. For example, we have found that sustained heating at 14.9 W resulted in a mass loss rate of $7.31 \times 10^{-9}\ \mathrm{g \cdot s^{-1} \cdot cm^{-2}}$ in a vacuum. From the available data on saturated vapor pressure of various elements, the rate of evaporation of metallic elements is well known as a function of temperature [10]. In fact, the rate of evaporation W is best expressed as follows:

$$\log_{10} W = A - BT^{-1} - 0.5 \log_{10} T + C, \tag{2}$$

where for chromium $A = 12.88$, $B = 1.756 \times 10^4$, and $C = -3.3760$. T denotes the temperature given in K. An independent measure of the ribbon temperature is then found from this evaporative mass loss rate. Under the heating condition, the ribbon temperature is 1090 ± 10 K. The smallness of the uncertainty in measured temperature is due to the fact that the saturated vapor pressure and the rate of evaporation derived from it is a very strong function of temperature.

We have confirmed that the heat loss by evaporation is completely negligible compared with the losses due to thermal radiation and conduction. The conductive losses at the two ends of the heated ribbon are quite readily computed. So can the thermal radiation loss be determined once

a reasonable estimate for the hemispherical emissivity, averaged over the full spectral range, is made. These losses, based on the temperature obtained from the evaporative mass loss, are found to be in reasonable agreement with the total ohmic heating power. We note that derivation of the ribbon temperature from the measured evaporative mass loss is based on the observation that the outermost layer of the heated surface is dominated by chromium and, therefore, the mass loss is primarily due to chromium evaporation. The rate of evaporation for nickel, which is given by Eq. (2) with $A = 13.28$, $B = 2.184 \times 10^4$, and $C = -3.3497$, is orders of magnitude smaller than that of the chromium at a given temperature.

5. ANALYSIS OF DEPTH-DEPENDENT EMISSIVITY AND TEMPERATURE

We have shown that each LPP ablation reveals a new surface of changing elemental composition. Clearly, this is responsible for the time-dependent change in the emissivity of the surface. The emissivity data in the literature are scarce and vary widely in their absolute magnitudes for a variety of practical reasons. Our present study presented here points to the lack of knowledge of the exact elemental composition of the specimens used in the earlier measurements as the basic contributing reason for the difficulty. However, the spectral emissivity of chromium is consistently larger than that of nickel. The ratio of the emissivity of chromium to nickel is 1.04 at 373.2 K and becomes 1.11 at their respective melting points [11, 12]. The depth-dependent temperature profile suggested earlier can be understood in part on the basis of the inevitable depth dependence of electrical resistivity of the Nichrome specimen.

The ratio of the electrical resistivity of chromium to that of nickel shows a reasonably consistent trend: 2.02 at 250 K, 1.83 at 273.2 K, and 1.03 at 900 K [10, 13, 14]. On the other hand, the electrical resistivity of Nichrome is an order of magnitude larger than that of either chromium or nickel over a wide range of elemental composition. The composition dependence of electrical resistivity means that there exists a gradient in ohmic heating rate as a function of depth from the surface and position on the plane of the Nichrome ribbon. When a thin near-surface layer has been removed by LPP ablation, the spectral emissivity is changed because the freshly exposed surface has a different elemental composition.

At the same time, the freshly exposed surface reveals a lower temperature due to larger electrical resistivity in the under layer. Notice also that the largest heat sink of the Nichrome ribbon is the two electrical terminal posts to which the ribbon is clamped. The largely linear temperature gradient near the terminal posts develops into a three-dimensional temperature

profile in the middle of the ribbon. We argue that this transition of the temperature profiles contributes to a development of the negative temperature gradient into the ribbon's interior for the simple reason that heat conduction takes place in large measure across the interior cross section of the ribbon rather than at the surface. Within a period of time, whose duration is dependent on the local temperature, the thermal emission intensity of the exposed surface relaxes back to the level of the adjacent undisturbed surface. This is due to thermal relaxation and in part because chromium is replenished at the surface by diffusion, both increasing the local emissivity and reducing the electrical resistivity. While the process of elimination allows no other likely explanations, we suggest that full-scale numerical code modeling will help clarify the mechanisms at play in the temperature profile issue.

6. DEPTH DEPENDENCE OF THERMAL DIFFUSIVITY

From the three sets of successive LPP emission spectra, shown in Figs. 2, 4a, and 4b, we have deduced the mass lost from the respective Nichrome ribbon surfaces. Figure 5 shows the masses removed per LPP ablation in microgram units under identical measurement conditions for the three Nichrome specimens, having different thermal history. In each case the mass data in essence show the relative thermal diffusivity as a function of depth from the surface. The three sets of mass loss data also compare the thermal diffusivity of one specimen to those of the two others in the group. All three specimens have been derived from the same stock of Nichrome ribbon and differ only in thermal state or heating history. The reasons are shown in Eq (1), which quantifies the roles of thermal diffusion (D_T), the heat of formation (H_f) and thermal motion (M) of the free elemental species in determining the amount of mass lost during a LPP ablation.

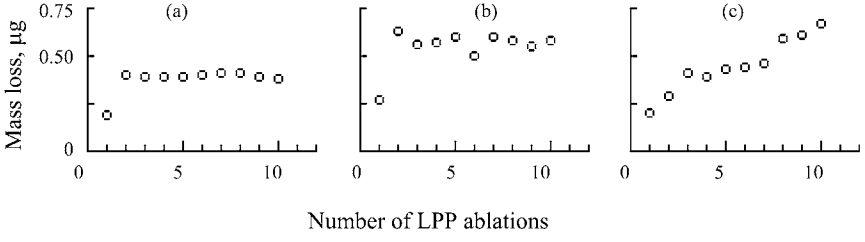

Fig. 5. Measured mass losses for the three Nichrome ribbons of Figs. 2, 4a, and 4b, respectively, as functions of the number of successive LPP ablation: (a) a fresh ribbon at room temperature, (b) a fresh ribbon at 1090 K, and (c) an aged ribbon at room temperature after 15 h heating at 1090 K.

Quantitative spectroscopy determines both the amount of target mass entrained into the LPP plume and the elemental composition of the plume unambiguously. The thermal velocity distribution of the constituent species in the plume is well prescribed. The heat of formation of the species that had resided within the ablation layer of the specimen's surface is affected by both the atomic properties and the morphology within the alloy layer, and is therefore subject to some interpretation. The morphology aspect in the determination of the heat of formation remains undetermined, and therefore we present the mass loss as a best measure of the depth dependence of thermal diffusivity at present.

No independent determination of the changes in the morphology of the ablation layer has been attempted, while the elemental compositions of the individual ablation layers have been fully characterized. Morphology characterization of a material specimen is a difficult task, and the kind of thermal diffusivity analysis presented in this paper may in fact help quantify the morphology once the composition effects in the development of the thermal diffusivity profile have been appropriately taken into account.

7. CONCLUSIONS

We have demonstrated that it is possible to surgically remove the surface contaminants by means of LPP ablation in a manner that exposes the local elemental composition. The thickness of the ablation layers to be removed can be controlled down to 50 nm per laser pulse [8, 9]. Time- and space-resolved spectroscopic analysis of the LPP plume composed of the matter from the surface of the specimen provides the elemental composition, making it possible to unambiguously connect the electrical, thermal, and radiative properties of the surface layer in question to its elemental composition. Theoretical and numerical models of the materials properties can now be effectively constructed on the basis of these two sets of measurements.

We have documented a case study of an 80Ni-20Cr Nichrome ribbon in regard to the effect of the removal of near-surface layers in succession on the thermal emission intensity when the ribbon is heated to 1300 K. At elevated temperatures, chromium has been found to diffuse preferentially to the surface, displacing nickel. This modifies in time both the emissivity and electrical resistivity of the heated Nichrome ribbon. In turn, the thermal emission intensity changes widely after each LPP ablation of the surface matter due to modest changes in both the emissivity and the local ohmic-heating rate.

The large disparity in the rates of evaporation of chromium and nickel and preferential diffusion of chromium to the surface have made it possible

to determine the temperature of the heated Nichrome ribbon from the measured rate of evaporative mass loss. The mass loss is attributed to chromium whose saturated vapor pressure is well established. The rate of evaporation derived from the vapor pressure data provides the link to temperature. It requires no calibration other than measuring the change of mass of the specimen after a period of heating in a high vacuum.

The process of surgically removing the surface layers by LPP ablation has a potentially very useful role to play in pulse heating studies of thermophysical properties. Contamination of the material surfaces by oxides has been noted as problematic in many studies [15]. Representative LPP ablation provides both the means to remove the surface contaminants and the confirmation that a surface of bulk elemental composition has been restored. The method is applicable to any state of the material specimen because it requires no contact with the specimen, and its implementation is simple, as it is effected entirely by optical means.

REFERENCES

1. Y. W. Kim, in *Laser-Induced Plasmas and Applications*, L. J. Radziemski and D. A. Cremers, eds. (Marcell Dekker, New York, 1989), Chap. 8.
2. Y. W. Kim, *High Temp. Sci.* **26**:57 (1990).
3. Y. W. Kim, in *Intelligent Processing of Materials*, H. G. N. Wadley and W. E. Eckhart, eds. (The Minerals, Metals and Materials Society, Warrendale, Pennsylvania, 1990), p. 317.
4. Y. W. Kim, in *Advanced Sensing, Modeling, and Control of Materials Processing,* E. F. Mattys and B. Kushner, eds. (TMS, Warrendale, Pennsylvania, 1992), p. 44.
5. Y. W. Kim and C. S. Park, *Int. J. Thermophys.* **17**:713 (1996).
6. Y. W. Kim, and C. S. Park., *Int. J. Thermophys.* **17**:1125 (1996).
7. Y. W. Kim, *Int. J. Thermophys.* **20**:1315 (1999).
8. Y. W. Kim, in *Thermal Conductivity 25/Thermal Expansion 13*, C. Uher and D. Morelli, eds. (Technomic Publishing, Lancaster, Pennsylvania, 2000), p. 15.
9. Y. W. Kim, *Int. J. Thermophys.* **14**:397 (1993).
10. D. E. Gray, ed., *AIP Handbook, 3rd Ed.* (McGraw-Hill, New York, 1972).
11. W. E. Forsythe, *Smithsonian Physical Table, 9th Ed.* (The Smithsonian Institution, Washington, 1954).
12. W. M. Rohsenow, J. P. Hartnett, and Y. I. Cho, *Handbook of Heat Transfer*, 3rd Ed. (McGraw-Hill, New York, 1998), Chap. 16.
13. H. E. Boyer and T. L. Gall, eds. *Metals Handbook* (ASM, Metals Park, 1985).
14. D. L. Lide, ed., *Handbook of Chemistry and Physics*, 75th Ed. (CRC Press, Boca Raton, Florida, 1994).
15. F. Righini, J. Spisiak, and G. C. Bussolino, *Int. J. Thermophys.* **20**:1095 (1999).